Contrast Agent Incorporation into Silicone Enables Real-Time Flow-Structure Analysis of Mammalian Vein-Inspired Soft Pumps

*Michael Loepfe, Christoph M. Schumacher, Cornelia H. Burri, and Wendelin J. Stark**

The construction of machines consisting essentially of soft parts is a nascent and multidisciplinary research field between material science, machine engineering, and robotics. Soft silicones represent a promising class of materials for the creation of a vast multitude of biologically inspired entities. In the present work, a new type of mammalian vein-inspired soft silicone pump is introduced and characterized, which is fabricated by virtual lost-wax casting of 3D-printed injection molds. These pumps can be actuated pneumatically or by internal gas combustion and preserve their functionality even after a freezing/unfreezing cycle. The possibility of using medical examination methods such as ultrasonic imaging to directly access flow information inside soft pumps is shown. Based on soda lime glass microspheres, a method is demonstrated to enhance contrast properties during such color online Doppler imaging for a detailed understanding of the inner fluid-structure interactions.

1. Introduction

Recent development in soft mechanics has yielded machines that are capable of performing very complex movements.[1] They can grab like a human hand, roll like a caterpillar or swim like a fish.[2] Powered by inflating pneu-net actuators, by applying voltage to shape memory alloys or by burning off hydrocarbons, soft machines can use many different actuation principles.[3] The soft principle can be further used to build more basic structures such as soft pumps.[4] These pumps offer several advantages compared with rigid machines, which work within dimensionally tight and preset boundaries. They are light weight and run even under deformational stress, without the need of a lubrication system. Regardless of the machine, all these systems take advantage of the elastomeric nature of their building material in order to generate actuation. However, none of these systems yet exploited silicone elasticity to gain further information on the running characteristics of these machines.

Noninvasive examination techniques are well known for soft tissues. Using magnetic resonance imaging (MRI), computer tomography or ultrasonography, medical professionals examine human tissue on a daily basis to explore the inner life of their patient's bodies. Especially, ultrasonic imaging is widely applied in medical care due to comparably low handling costs and versatile applicability (i.e., most parts of the human body can be investigated). Ultrasonography is also part of the online-monitoring equipment during heart surgery.[5] There, these devices take advantage of the Doppler Effect to detect flow within the scanned area. So-called color Doppler imaging (CDI) forms a standard procedure to evaluate the integrity of i.e., a heart valve by measuring any undesirable backflow. Research has already combined this technique with computational fluid dynamics (CFD). CDI delivers reliable flow information, which can be implemented as boundary conditions into numerical models of CFD calculations.[6] Nevertheless, these investigations yet only focused on biomedically relevant systems, such as mitral regurgitation (insufficiency of the left atrioventricular valve to close properly). Combining medical imaging with traditional soft mechanics would therefore create a technique, allowing the gain of flow information for directly applicable systems.

Medical professionals train many years in order to measure, analyze, and interpret obtained data of such noninvasive imaging methods. One of their main focuses in ultrasonography is the development of the spatial sense to recognize tissue structures, nerves blood vessels or bones during an examination session.[7] To facilitate interpretation, contrast agents are widely applied.[8] Introduced into a patient, they enhance backscattering due to material properties of the contrast agent. Usually, vessel-rich body parts benefit from this enhancement, because the fluid phase contains the contrast agent. However, this enhancement could also take place in an elastomeric phase, enhancing wall contrast. This would allow better recognition of elastomer movement in soft actuation, especially for untrained examiners.

In this work, we demonstrate the successful flow analysis inside a soft pump by CDI after contrast agent incorporation into elastomer, as well as reliable fluid pumping using different pump actuation patterns. Based on lost-wax casting of virtually designed and 3D printed injection molds, we produce a soft pump analogue inspired by the functionality of mammalian veins.[4b,4c,9] Our modular mold approach enables production

M. Loepfe, Dr. C. M. Schumacher, C. H. Burri, Prof. W. J. Stark
Institute for Chemical- and Bioengineering
Vladimir-Prelog-Weg 1, 8093 Zurich, Switzerland
E-mail: wendelin.stark@chem.ethz.ch

DOI: 10.1002/adfm.201404461

of monoblock pumps with different, segmented length (up to 80 cm), approaching the general design of a human vein (i.e., several valves inside an entire vein). Incorporation of a simple contrast agent modifies the used room temperature vulcanizing (RTV) silicone elastomer, and thereby enhances imaging properties. This modified silicone is then injected into the molds. Actuation by internal gas combustion or by pressurized air is evaluated for a reliable pumping. We image internal flow at common actuation regimes by CDI for different pumping fluids, such as water, silicone oil, ketchup or starch-water mixture. Simple parameter analysis evaluates the impact of pump frequency and pressure on the obtained pump rate, optimizing the soft system to pump up to 5 m of height at a flow of over 500 mL min^{-1}.

2. Design of Venous Soft Pump Analogue

Blood vessels are commonly examined by medical professionals using ultrasonic imaging. We designed a vein-like soft pump, capable of peristaltic pumping of fluids. This pump follows the same pumping principle as in mammalian veins (**Scheme 1**.). Upon relaxation of adjacent muscles or pulsating arteries, the squeezed vein creates a slight vacuum. The vacuum then forces the valve lips facing the squeezed vein section to open. This segment fills with blood until pressure difference is equalized or another contraction incident occurs. Such a contraction incident squeezes the vein again and increases the pressure inside. The valve facing its lips toward the pressurized segment now closes. The other valve is forced to open and thereby expulses blood into the next vein section. Refilling of one segment is usually supported by expulsion of an adjacent segment, enabling this passive transport.

Our pump comprises a pressure chamber, which imitates the contraction of adjacent muscles or pulsating arteries (Scheme 1b, Supporting Information). This chamber jackets the tubular pump chamber, leaving space for a thin actuation membrane within (Figure S1, Supporting Information). Upon a pressure increase inside the pressure chamber (by pneumatics or by gas combustion), the fluid phase is squeezed like in a mammalian vein. Adjacent valves with similar, natural shape then guide the flow. Subsequent pressure release (i.e., by pressure relief valve opening) relaxes the soft pump and allows refilling of the fluid chamber (Figure S2, Supporting Information). For direct inflation of the pressure chamber, aramid fabrics are used as an outer shell. The pump can be driven by pneumatic expansion or gas combustion. In both cases, a programmable logic controller (PLC) controls valves (and respectively an electric spark ignition for gas combustion operation). Since we are mainly going to use pneumatics to power this soft pump, we explain its design more in detail. In a relaxed state, the pump has closed inlet- and open outlet pressure chamber valves. When the PLC triggers a pumping pulse, the inlet valve opens and the outlet valve closes. The jacket now fills for a preset time and pressure. This consequently increases fluid pressure and expels the pump fluid as described above. To relax, the PLC closes or opens inlet and outlet valves, respectively. The jacket relaxes and fluid pressure decreases (Further details on the design and combustion actuation are given in the Supporting Information).

Our blood vessels usually contain several valves within a limb. For instance, the great leg vein, *V. saphena magna*,

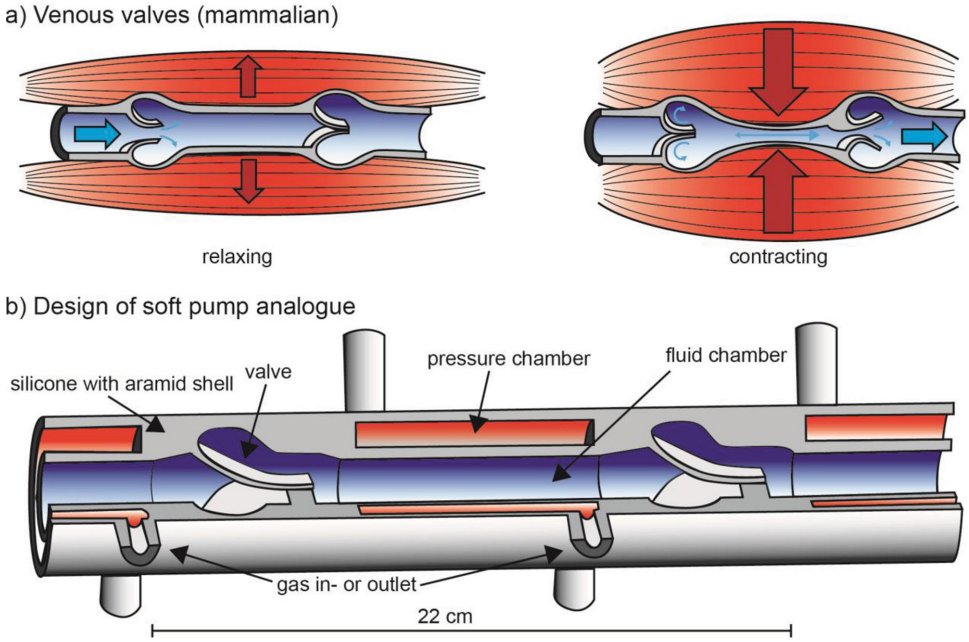

Scheme 1. a) Operating mode of mammalian veins. Upon relaxation of adjacent muscles or pulsating arteries, a slight vacuum is created inside a vein segment (a, left). This leads to an opening of the valve lips, facing the segment of interest. The segment is now filled again with blood. Subsequent muscle contractions or artery pulses then also contract the venous segment again (a, right). The increasing pressure forces the left valve (facing the segment) to close, whereas it pushes the right valve (valve lips point to next segment) to open. b) Design of our soft pump analogue. The fluid chamber (lumen) contains vein-like valves. Contraction of muscles or artery pulses is simulated by a pressure chamber, which can be driven pneumatically or by gas combustion.

contains roughly eight valves in an adult person.[10] One of our pump designs therefore consists of several pump segments to mimic such veins. Recently, we produced soft pumps by injection of RTV silicone mixtures into 3D-printed molds, designed by virtual lost-wax casting.[4b,4c] For this soft machine type however, pump size would be limited to available 3D printing dimensions size. Thus, we designed valve modules and pump modules, which can be assembled together in a repetitive way to form a larger injection mold (see Figures S1–S7, Supporting Information, for details). These molds can be filled with modified silicone containing a contrast agent. The contrast agent enables enhanced imaging properties for noninvasive examination techniques, such as medical sonography or MRI.

3. Results and Discussion

3.1. Silicone Modification

The most important effect of contrast agents in medical sonography is their ability to enhance backscattering (echogenicity). This is usually achieved by introduction of free or encapsulated gas bubbles, colloidal suspensions or emulsions, which can be applied intravenously. These agents effectively increase scattering cross-section of a small scatterer, which is given by the expression from Ophir et al.[11]

$$\sigma = \frac{4\pi}{9} k^4 a^6 \cdot f\left(\kappa_s - \kappa, \rho_s - \rho\right) \tag{1}$$

where $k = 2\pi\lambda^{-1}$ = wave number and λ is the wavelength; a = radius of scatterer, much smaller than $\lambda\kappa$ = compressibility difference between scatterer and tissue; and ρ = density difference between scatterer and tissue.

Since we want to incorporate contrast agents to increase echogenicity of our soft pumps, our agents should be simple and manageable for silicone modification. Gases are very well soluble in silicone and would correspondingly hinder a size-controlled incorporation of gaseous contrast agents.[12] Further, our modification should not negatively influence material properties. Otherwise we would create soft pumps, which would not reflect the actual behavior of the structure and the material upon actuation. Modifying agents should therefore be low concentrated in order to maintain material properties. Thus, fluid–fluid or fluid–solid systems might be challenging as well, because properties are likely to get lost during incorporation (i.e., phase dilution).

Spherical soda lime glass beads are a simple and manageable contrast agent. For such solid back scatterer (i.e., $\kappa_s << \kappa$ and $\rho_s >> \rho$), this function term reduces to a single-digit value, which simplifies Equation (1) to

$$\sigma \approx a^6 \tag{2}$$

when we measure at a constant wave length. The effective scattering cross-section then results from the number of scatterers, m and the individual scattering cross-section σ

$$\sigma_{eff} = m \cdot \sigma \rightarrow \sigma_{eff} \approx m \cdot a^6 \tag{3}$$

In other words, our contrast agent needs to be as large as possible to get good echogenicity but also as diluted as possible to maintain material properties. It becomes obvious that there is a size optimum of the used beads.

This size effect is shown in **Figure 1**, where we recorded sonograms of soft silicone with different bead loadings and sizes. We immediately see that for a given size, backscattering decreases for smaller bead concentrations. Further, we observe decreased backscattering for decreasing bead sizes (Figure 1b–d) as Equation (3) suggests. This trend is best

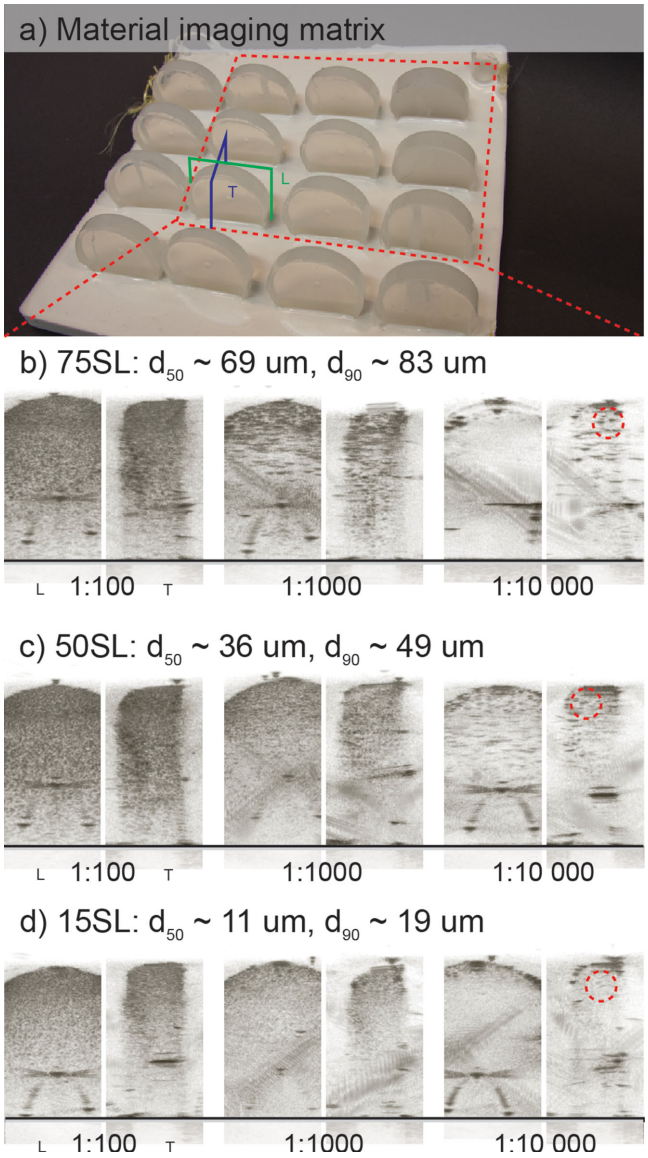

Figure 1. a) Embedded material test specimens are shown for backscattering analysis. Selected data is illustrated with a red dashed square. Longitudinal (L) and transversal (T) imaging planes are indicated on a test specimen. b–d) Recorded sonograms for different particle sizes at different bead loading. For a better visualization, recorded scans were inversed in grayscale. Solid, black line represents immersion depth of specimen embedment. Dilution factors are given per mass of prepolymer used. Dashed red circle illustrate achieved backscattering by single particles.

Table 1. Results of stress–strain test for silicone with and without soda lime glass beads incorporation. Data was obtained according to DIN 53504 and for a sample number of $n = 5$.

Sample	Stress [MPa]	Strain [%]
Silicone	0.79 ± 0.13	674 ± 67
Silicone with SL75 beads	0.83 ± 0.12	680 ± 87

observed by considering a single particle (i.e., at high dilution) to see its actual backscattering. Hence, we have demonstrated successful incorporation of soda lime glass beads into silicone to control backscattering for ultrasound imaging. However, the mechanical properties should not change significantly as mentioned earlier. From the obtained backscattering matrix (Figure 1), we therefore concluded that the largest bead size (SL75) at a concentration of 0.1 wt% per mass of prepolymer would suit best for our purposes. We therefore tested tensile properties according to DIN 53405 for unmodified and modified silicone (Figure S8, Supporting Information). The results of this test are shown in **Table 1**. No significant changes of the tensile strain properties were found. A two-tailed *t*-test further showed no deviations for a significance level of 5%. Therefore, we can conclude that the material modification does not substantially change our systems and we can expect comparable acting of our soft pumps upon imaging.

3.2. Ultrasound Imaging and Flow Visualization

Powering soft pumps by pneumatics or by gas combustion has deviating consequences for subsequent analysis. Combustion results in sharp pressure increases, which can however not be maintained for long time periods (less than 10 ms).[3h] Pneumatic actuation therefore results in different actuation behavior. The pressure increase takes much longer due to mass transport limitation imposed by the small pressure chamber inlet diameters, but the pressure can be kept for long time periods due to the isothermal behavior. In order to visualize these effects, we pumped to a hydrostatic head of 2 m using a single segmented pump, either driven by methane combustion or compressed air. Gravimetrical flow analysis for a pump frequency of 0.5 Hz showed that pneumatics performed superior (4.4 g s^{-1}) compared with gas combustion (1.5 g s^{-1}). Hence, we focused on pneumatically driven systems in this work, allowing a simpler control mechanism (for details, see Supporting Information).

Being able to modify soft silicones by incorporating soda lime glass beads (**Figure 2**), we focused on ultrasound imaging. A simple material test valve was designed, which can be actuated by manual squeezing of a bulb-shaped posterior part (Figure S9, Supporting Information). Upon actuation, sonography is able to record all valve movements. Imaging was performed in a water bucket containing 500 ppm of liquid soap. The soap changes water surface tension and correspondingly reduces air bubble attachment on silicone (i.e., less signal attenuation). The array transducer was placed in such a way that the imaging plane results in a cut through the valve axis (Figure 2b). We were able to observe valve movement by squeezing the bulb (Video S1, Supporting Information).

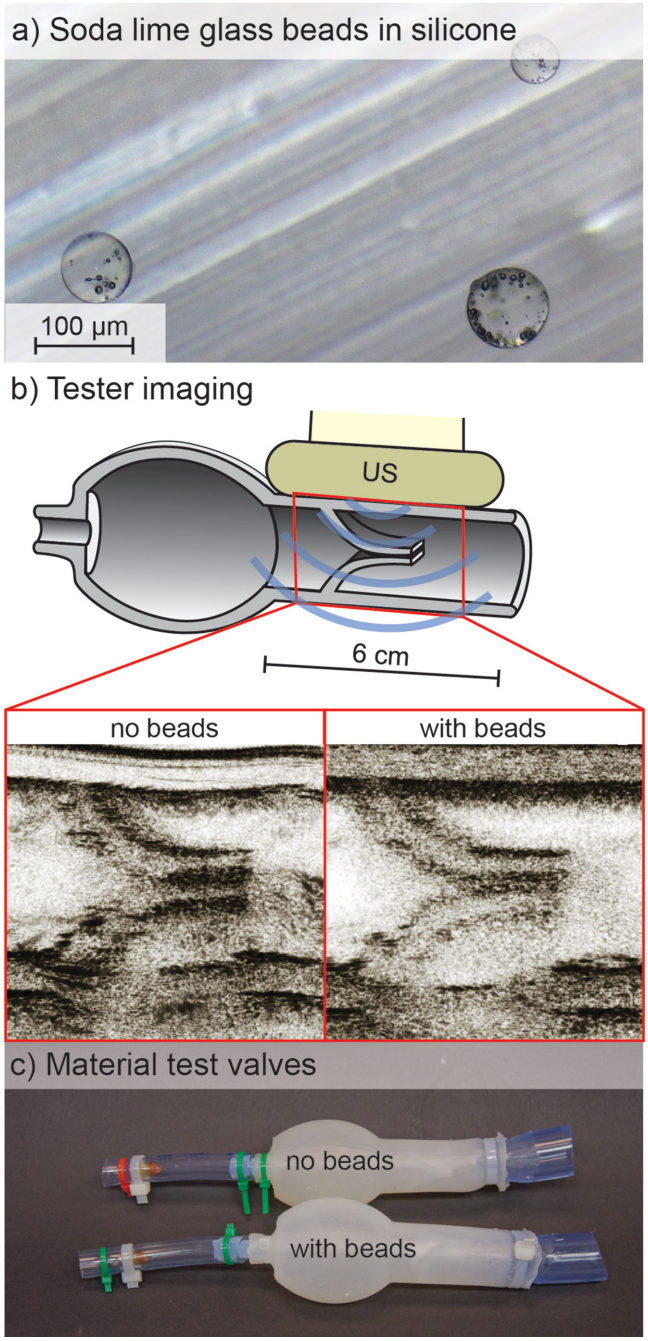

Figure 2. a) Reflected-light microscopy images of incorporated soda lime glass beads in silicone. For a better visualization, several slices were recorded to form a z-stack projection of the material. b) Cross-section scheme of the material test valve design is shown with further illustration of the imaging process. The bulb part of the tester can be used to manually pump fluid trough the tester. Sonograms of material testers with and without incorporated beads are shown in the red squares below. Increased backscattering is observed within material walls compared with unmodified silicone. c) Material test valves are shown with all additional connections (check valve and positioning tubing).

Ultrasonic scans showed again that our silicone modification with contrast agent increased backscattering. This can be seen by comparing the wall contrast for modified and unmodified

silicone (Figure 2b,c). We further analyzed contrast in the motion mode (M-mode). This technique resolves a single pixel line in time and thereby gives insight into the motion behavior of a moving system (i.e., a valve flap). We again observed increased backscattering in 2D-mode, which helped to identify a promising movement. After switching into M-mode, the observation was focused on the movement and therefore, the increased backscattering was less important (Figure S10, Supporting Information).

As already mentioned in the introduction, the Doppler effect can be used to visualize flow dynamics in soft tissues. Depending on incident, backscattered waves, flow speed, and direction can be assigned (flow toward or away from the probe section). A color map then visualizes this information on the recorded 2D image in real time for a chosen section. We applied this standard medical examination technique to our soft pumps. The material tester was investigated at different squeezing velocities. Color Doppler recordings show different linear velocities, which cope well with applied squeezing (Video S2, Supporting Information). Hence, flow visualization is possible for our small sized material test valves.

Our aim however is to visualize flow in larger pumps. We performed ultrasound imaging and flow visualization for a single segmented version. This version has not yet the size of the final multisegment pump, but already uses the same valve and basic pump design (**Figure 3**). The single segment also delivers reasonable flow information on internal currents during pumping action (**Figure 4**). Regions of interest for venous flow analysis are, besides junctions, located directly after a valve. In mammalians, currents can create blood stagnation at these locations that may support formation of varicose veins.[13] This is why we also expect most interesting flow currents in the region of the vein pocket, located after the valve.

We evaluated flow characteristics for different fluids (i.e., water, silicone oil, ketchup, and starch-water mixture) to get further understanding of fluid properties impacting our pump characteristics. Water pumping showed the fastest currents with a linear velocity of roughly 6 cm s^{-1} (Figure 4a). Video evaluation suggests that there is only a single current zone induced by the valve movement within the pocket (Video S3, Supporting Information). When the valve is pushed open by a pressure front, the adjacent fluid elements in the pocket give way by moving on one single side. Subsequent wall relaxation then turns pocket currents around. Another good impression of flow characteristics is again given by the M-mode to gain insight into the motion behavior of a valve. We did observe sharp and symmetrical pulse amplitudes with a relaxation width (i.e., dead time) of roughly 0.5 s between two pulses. This suggests that the pump frequency might be increased to have less dead time between two contractions. Also, symmetrical pulse characteristics suggest good valve opening and closing time (i.e., silicone valve can open and close without experiencing severe resistance by the fluid).

By increasing fluid density and viscosity (i.e., pumping silicone oil), we observe decreased linear velocities only up to 4 cm s^{-1} (Figure 4b). Also, there seems to be a second current zone close to the pocket neck with an inversed flow (Video S3, Supporting Information). The recorded motion line showed an unsymmetrical pulse shape, flattening on the right-hand side

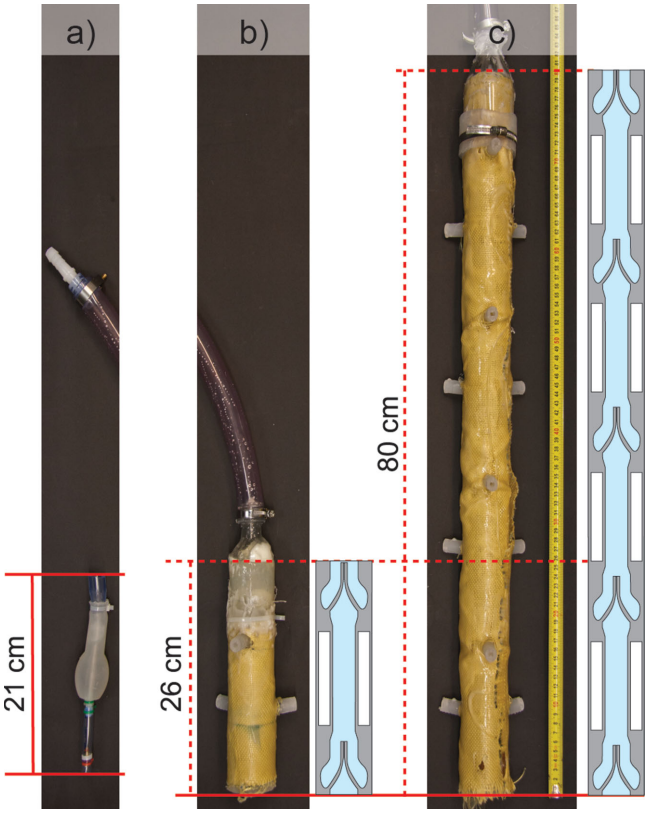

Figure 3. Overview on the produced soft pumps. a) Material test valve designed for initial imaging tests. b) Single segment venous soft pump analogue with schematically visualized cross-section. The upper valve part has no reinforcing fabric layer to allow direct application of the ultrasonic transducer array on the pump. c) Quadruple-segmented venous soft pump analogue with schematically visualized cross-section.

with no observable dead time. Hence, pumping frequency is at an optimal point but the flattening suggests improving of the valve design for fluids with higher viscosities (i.e., increasing valve stiffness) to enable faster closing times. Pumping nonNewtonian fluids revealed further flow characteristics (Figure 4c,d). Ketchup, a shear-thinning fluid, showed even lower linear velocities up to 2 cm s^{-1}, while again observing a second current zone (Video S3, Supporting Information). Pulse profiles were flat but symmetrical, thereby suggesting that the pump had difficulties to displace fluid elements in the valve pocket. Dead time was estimated to be roughly 1 s, thus frequency could have been increased to 1 instead of 0.5 Hz. We observed similar flow characteristics for a shear-thickening starch–water mixture. A starch–water mixture incorporates many small starch grains, which cause a lot of signal attenuation. For this reason, it was difficult to penetrate deeply into the soft pump while imaging.

Even though our flow analysis is rather approximate than detailed, we were able to gain real-time insight into the soft pumps. We strongly believe that with further improvements, considerably wider comprehension could be possible. This would be of great interest to research areas employing CFD and fluid-structure interaction. Usually their computational models are in need of appropriate boundary conditions in order to

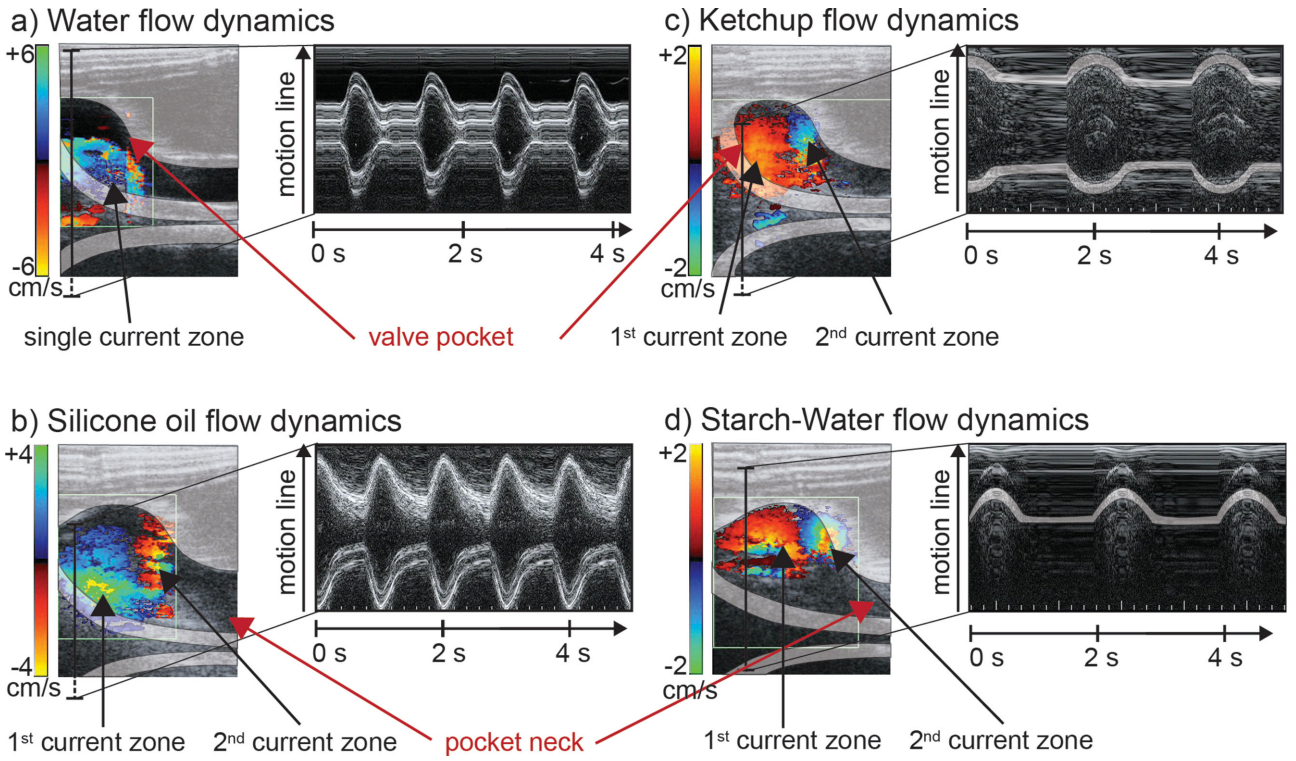

Figure 4. Flow visualization in a venous soft pump analogue using color Doppler imaging. The region of interest is set to the valve pockets, where most interesting currents are expected. For a better understanding, pump walls and valves are highlighted by a schematic, semitransparent layer. a–d) show flows of different pump fluids. Valve movement is shown on the right side of each fluid system by a time-resolved motion line. Flow dynamics of a) water and b) silicone oil (both Newtonian fluids) are shown at a pump frequency of 1 Hz. NonNewtonian fluids as c) ketchup and d) starch–water mixture were pumped at a lower frequency of 0.5 Hz.

converge. By designing soft analogues of the systems of interest (i.e., industrial valves), this information would be accessible. Combining CFD with noninvasive flow measurements was so far performed for medically relevant systems, such as heart support systems.[14] We hereby show that data can also be obtained by CDI for venous soft pump analogues and more generally in soft machines through the incorporation of contrast agents into elastomers.

3.3. Peristaltic Pumping of Venous Soft Pump Analogue

In order to investigate pumping of the four segmented soft pump, we pumped water to a hydrostatic head of 2 m by applying different pressure chamber actuation patterns and conditions.[4a] As already mentioned, gas valves were controlled by a PLC, allowing simple modification of the pump patterns. First, we analyzed two-segment patterns with single gas in- and outlet, as well as filling and ventilation times of 25% and 75% per pulse interval, respectively. These patterns consisted of subsequent or simultaneous actuation of two segments inside the four segmented soft pump. To facilitate cycle understanding of the segments, we hereby introduce an (X-X-X-X) nomenclature.[4a] Each X represents a pump segment to which, number values are assigned according to their relative actuation moment within a cycle. Therefore, the subsequent, two-segment pattern within a four segmented pump would have the notation (1-2-1-2). The simultaneous pattern would have the notation (1-1-2-2). We then evaluated mass pump rate by gravimetrical analysis for pneumatic pressures of 0.7–2 bars with pump frequencies of 0.5, 1 or 2 Hz (**Figure 5**a). Flows were normalized by the pump frequency to get mass flow rates per pump beat.

We observed that the (1-1-2-2) pattern mostly results in higher pump rates than the (1-2-1-2) pattern, regardless of applied pressure and frequency. This might be explained by a beneficial interaction of the two adjacent pump segments for the (1-1-2-2) pattern. There, the interconnected valve might not seal completely upon contraction and thus extends the pumping segment. However, at a pressure/frequency-configuration of 1.5 bar and 0.5 Hz, the (1–1–2–2) pattern had lower mass flow rates than the (1–2–1–2) pattern. Since all pumping rates were measured fivefold with a corresponding measurement deviation of typically lower than 1% (for flow rates larger 2 g beat^{-1}), these phenomena are significant. A possible explanation might be that the interconnecting vein valve now starts to seal more rigorously due to an increased fluid pressure and thereby, prevents any additional fluid exchange during the compression phase (such that segment extension is annulled). M-mode analysis of the interconnected valve then helped to identify that the flap opens more violently when pumping with the (1-1-2-2) pattern than for the (1-2-1-2) pattern (Figure S11, Supporting Information). This can be explained by the pressure increase resulting from the upper segment due to the simultaneous

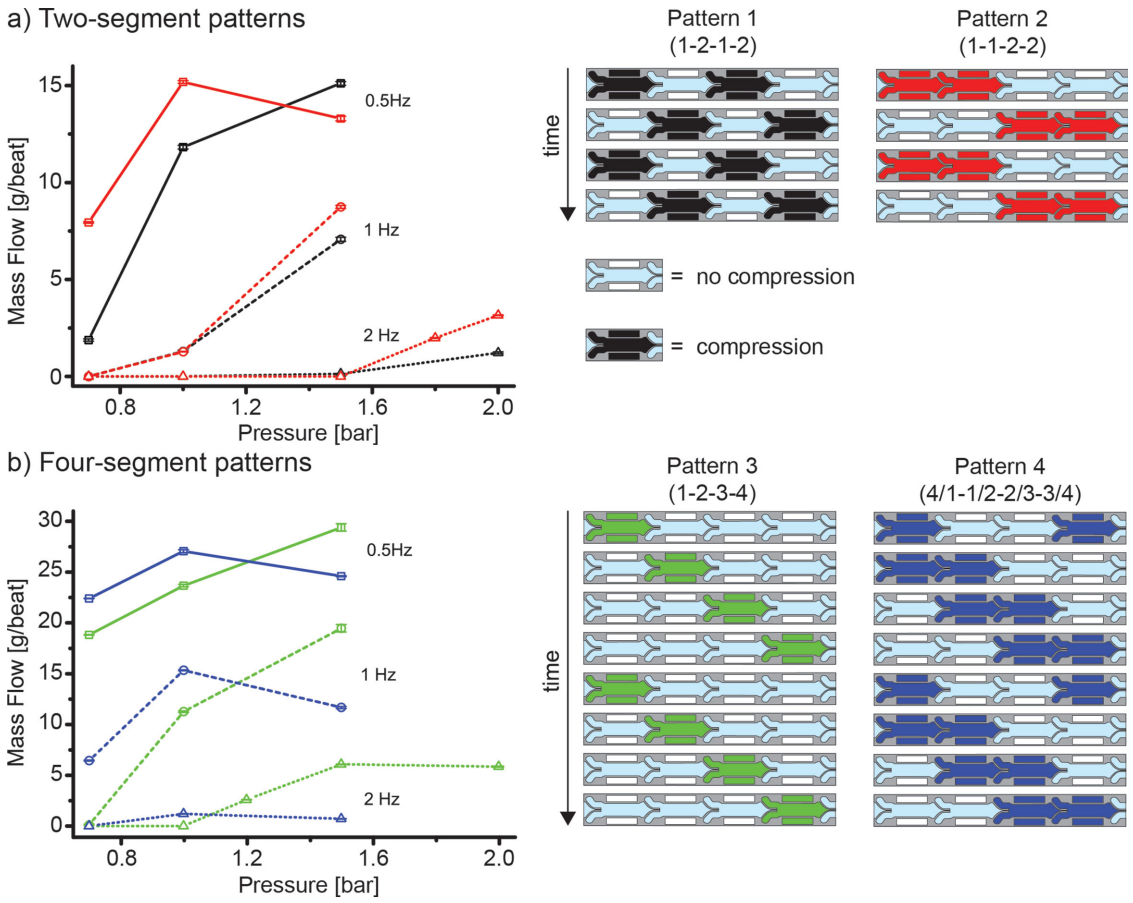

Figure 5. Influence of pressure and pump frequency on mass pump rate is shown for two and four-segment pump patterns. Single in and outlet was used with filling and ventilation times of 25% and 75% per pulse interval, respectively. All measurements were taken fivefold. Resulting standard deviations are indicated in the two plots. a) Two-segment patterns are shown for a subsequent (1–2–1–2) and simultaneous (1–1–2–2) segment actuation. Visualization for both patterns is given on the right. b) Four-segment patterns are shown for direct (1–2–3–4) and for an overlapping pulse propagation (4/1–1/2–2/3–3/4). Pattern visualization is again given on the right.

contraction. Thus, the valve is closed more rigorously and has a delayed opening, which also reduces the pump rate. The compression phase at 0.5 Hz takes 0.5 s (25% fill time per 2 s cycle) and is therefore the longest amongst all frequencies. A higher pneumatic inlet pressure also favors a higher final jacket pressure, thus increasing fluid pressure as well. Nevertheless, the beneficial segment interaction of the simultaneous pattern also suggests that the fluid needs a start-up time to reach higher pump rates.

To reach longer flow start-up times, we switched to four-segment pumping. Two possible patterns were evaluated. The first pattern used a pulse propagating through the entire four segments of the pump (1–2–3–4), whereas the second pattern should take advantage of pulse overlapping. This leads to the notation (4/1–1/2–2/3–3/4), which is also illustrated in Figure 5b. The impact of extended flow start-up times is clearly observable by comparing two-segment and four-segment patterns. We observed much higher flow rates for the same pressure and frequency condition. Further, a drop in mass pump rate was observed for the pulse overlapping pattern (4/1–1/2–2/3–3/4) at elevated pressures, regardless of the pump frequency. This might again be a pump sealing effect, where the interconnected vein valve is closed upon a higher inlet pressure as mentioned earlier. Hence, the pulse propagation pattern without overlapping (1–2–3–4) seems to be the best pattern for pumping. We then tested, if the soft machine was still able to pump upon bending. Our measurement showed that pumping was still possible with less than 10% decrease in efficiency for a bending angle of 26°.

Another interesting observation can be made by comparing pump rates at a given pressure for pattern (1–2–3–4). Before, we would like to emphasize again that pump flow rates are given per actuation cycle with units of g beat^{-1}. This allows a better comparability in terms expulsion effectiveness. At a pneumatic pressure of 1.5 bar and a frequency of 2 Hz, we observed approximately 6 g beat^{-1}. If a linear dependence of the frequency and pump rate should apply, the pump rate per beat could double for the half frequency (1 Hz) at the same pneumatic pressure. However, we observed a much higher rate (19.5 g beat^{-1}). If we further have the frequency, the rate should reach approximately 40 g beat^{-1} but measured flow rate was much less (29 g beat^{-1}) for a frequency of 0.5 Hz. Therefore, an optimum is expected where pumping frequency meets best elastic material properties of the venous soft pump analogue.

A simple way to increase pneumatic start-up times further is performed by adding a second pressure chamber gas outlet. This allows longer liquid filling time frames without the risk of gas accumulation, causing the pump to collapse (i.e., permanent sealing of pump chamber). We therefore changed the filling and ventilation times to 50% each per pulse interval. Further, pump height was increased to 5 m to generate demanding operation conditions (i.e., pumping from a flooded basement). Again, we measured at different frequency/pressure-configurations to screen for an optimal operation parameter set (**Figure 6**, Video S4, Supporting Information). Since we are interested in the overall performance, pump rates are now given in g s^{-1}. We observe a local maximum around a frequency of 1.25 Hz and a pressure of 1.8 bar, yielding a flow rate of 8.75 g s^{-1}. The shape of the frequency plane of 1.25 Hz clearly shows that there seems to be an optimal operation point, where pump actuation and material characteristics best match together.

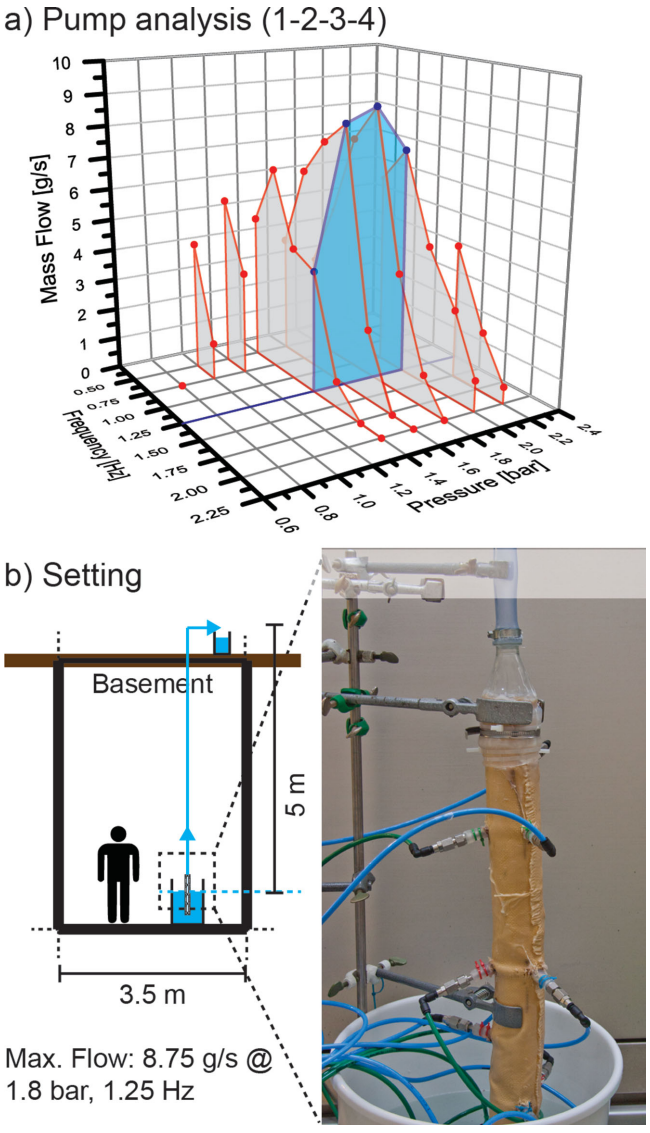

Figure 6. a) Detailed investigation of parameter impact on mass pump flow rate is shown for a frequency range of 0.5–2 Hz and pneumatic pressures of 0.8–2.2 bar for the (1–2–3–4) pump pattern. To increase flow start-up times, two exhausts were used with filling and ventilation times to 50% each per pulse interval. The frequency plain containing the highest mass flow rate is further emphasized with blue points. Only one measurement was taken per frequency/pressure-point due to previously shown very small measurement errors. b) The pump setting is shown for this parameter investigation. The inset shows the installed four-segment venous soft pump analogue.

With the obtained knowledge, we are able to classify the pump design and compare its properties to already available systems. The presented design entirely separates pump fluid and actuation jacket. Due to this partition, the pump requires no sliding planes, which usually need extensive care to minimize damage caused by small debris in the fluid (i.e., a filter unit to remove debris in oil pumps). Thus, the mammalian vein-inspired soft pump can be compared with traditional peristaltic pumps. However, the pump has a substantial difference in terms of manufacturing and storing. The injected silicone not only produces lightweight and elastic pumps but also has other consequences based on this material choice. Silicones are known to have high elongation at break, are UV and temperature insensitive (i.e., –20 to 300 °C without loss of elasticity), and are moisture resistant.[4b,4c,15] Therefore, our soft machine was still able to pump after the frozen fluid phase had melted again (Figure S12, Supporting Information). This could be useful, where low weight and good storage properties are required (i.e., on-site pumps in buildings of possible flooding areas or outdoor pumps, where temperature is likely to drop below 0 °C).

The presented pump design can be further improved, particularly if comparing its weight (2.1 kg for a four-segment pump) and its energy efficiency (1%, see Supporting Information for detailed calculations) to the resulting pump rate (500 mL min^{-1}) and head (5 m, corresponding to 0.5 bar). Nevertheless, these facts should again be compared with the resulting robustness, the storage properties and the ability of real-time flow analysis within a soft pump design.

4. Conclusion

The application of the recently presented virtual lost-wax casting technology using RTV soft silicones has opened versatile perspectives toward soft machines and robots with complex geometries. A key advantage of these machines is that they are essentially made from one single part. This avoids weak spots caused by material discontinuities such as bonding surfaces. In this work, we thoroughly investigated the characteristics of single- and multi-segment mammalian vein-inspired soft pumps with a special focus on real-time analysis of the inner workings regarding fluid-structure analysis. Based on mold stacking, we were able to show successful production of single part pumps with different segment lengths (up to 80 cm).

We managed to operate our pumps both by gas-combustion as well as pneumatically and introduced the concept of in situ observation of such systems by the use of well-established medical tools such as ultrasonic imaging. In order to enhance the observability of flow phenomenon and mechanical operation principles, we modified the used soft silicones with suitable contrast agents (soda lime glass microspheres). The specific

pump capabilities are dependent on the mechanical properties of the used soft material as well as external input parameters, such actuation patterns, frequency, and pressurization. Hence, we conducted detailed parameter optimization studies to find ideal operation constraints.

Due to the use of silicone, we can further exploit material properties (i.e., UV and temperature insensitivity, as well as moisture resistance) to identify a potential field of application, where long lasting and light weight properties are required even under low temperature conditions (i.e., on-site pumps or outdoor pumps). Driving such pumps by combustion instead of pressurized air might lead to further improvement due to the higher energy density of hydrocarbons. This would also lead to a direct pumping because the combustion would occur in the pressure jacket, which is adjacent to the fluid chamber.

Our findings point out the potential of structure pervading imaging tools after simple material modification for a deeper understanding of the inner motions of soft machines. Such information was before only accessible by numerically expensive calculations and did not represent the actual motion behavior (i.e., based on boundary values and model simplifications). This helps to shape future optimization strategies and design approaches for an interdisciplinary research field in material science, computational science, and mechanical engineering.

5. Experimental Section

Please see the Supporting Information for details of the experiments.

Supporting Information

Supporting Information is available from the Wiley Online Library or from the author.

Acknowledgements

Financial support by ETH Zurich is kindly acknowledged. The authors gratefully acknowledge the financial funding by the Baugarten Stiftung. This work is part of the Zurich Heart Project and is supported by Hochschulmedizin Zurich.

Received: December 17, 2014
Revised: January 29, 2015
Published online: February 25, 2015

[1] a) S. Kim, C. Laschi, B. Trimmer, *Trends Biotechnol.* **2013**, *31*, 287; b) A. Albu-Schaffer, O. Eiberger, M. Grebenstein, S. Haddadin, C. Ott, T. Wimbock, S. Wolf, G. Hirzinger, *IEEE Robot. Autom. Mag.* **2008**, *15*, 20.

[2] a) A Novel Type of Compliant, Underactuated Robotic Hand for Dexterous Grasping, R. Deimel, O. Brock, presented at RSS, Berkeley, USA **2014**; b) B. Mosadegh, P. Polygerinos, C. Keplinger, S. Wennstedt, R. F. Shepherd, U. Gupta, J. Shim, K. Bertoldi, C. J. Walsh, G. M. Whitesides, *Adv. Funct. Mater.* **2014**, *24*, 2163; c) L. Huai-Ti, G. L. Gary, T. Barry, *Bioinspir. Biomim.* **2011**, *6*, 026007; d) A. D. Marchese, C. D. Onal, D. Rus, *SoRo* **2014**, *1*, 75; e) J. Zhang, J. Tang, J. Hong, T. Lu, H. Wang, in *Intelligent Robotics and Applications*, Springer, International Publishing, Switzerland **2014**, 320.

[3] a) R. F. Shepherd, F. Ilievski, W. Choi, S. A. Morin, A. A. Stokes, A. D. Mazzeo, X. Chen, M. Wang, G. M. Whitesides, *Proc. Natl. Acad. Sci. U.S.A.* **2011**, *108*, 20400; b) R. F. Shepherd, A. A. Stokes, R. M. D. Nunes, G. M. Whitesides, *Adv. Mater.* **2013**, *25*, 6709; c) F. Ilievski, A. D. Mazzeo, R. F. Shepherd, X. Chen, G. M. Whitesides, *Angew. Chem.* **2011**, *123*, 1930; d) S. A. Morin, S. W. Kwok, J. Lessing, J. Ting, R. F. Shepherd, A. A. Stokes, G. M. Whitesides, *Adv. Funct. Mater.* **2014**, *24*, 5541; e) S. A. Morin, Y. Shevchenko, J. Lessing, S. W. Kwok, R. F. Shepherd, A. A. Stokes, G. M. Whitesides, *Adv. Mater.* **2014**, *26*, 5991; f) T. P. Chenal, J. C. Case, J. Paik, R. K. Kramer, Conformable Actuation and Sensing with Robotic Fabric, presented at, Conformable Actuation and Sensing with Robotic Fabric, presented at IROS, Chicago, USA, September, September, **2014**; g) G. Kofod, W. Wirges, M. Paajanen, S. Bauer, *Appl. Phys. Lett.* **2007**, *90*, 081916; h) R. F. Shepherd, A. A. Stokes, J. Freake, J. Barber, P. W. Snyder, A. D. Mazzeo, L. Cademartiri, S. A. Morin, G. M. Whitesides, *Angew. Chem. Int. Ed.* **2013**, *52*, 2892; i) M. T. Tolley, R. F. Shepherd, M. Karpelson, N. W. Bartlett, K. C. Galloway, M. Wehner, R. Nunes, G. M. Whitesides, R. J. Wood, An Untethered Jumping Soft Robot, presented at, An Untethered Jumping Soft Robot,presented at IROS, Chicago, USA, September, September, **2014**.

[4] a) R. Fuhrer, C. M. Schumacher, M. Zeltner, W. J. Stark, *Adv. Funct. Mater.* **2013**, *23*, 3845; b) M. Loepfe, C. M. Schumacher, W. J. Stark, *Ind. Eng. Chem. Res.* **2014**, *53*, 12519; c) C. M. Schumacher, M. Loepfe, R. Fuhrer, R. N. Grass, W. J. Stark, *RSC Adv.* **2014**, *4*, 16039; d) A Soft Combustion-Driven Pump for Soft Robots, C. Stergiopulos, D. Vogt, M. T. Tolley, M. Wehner, J. Barber, G. M. Whitesides, R. J. Wood, presented at *SMASIS, Newport, USA* **2014**; e) C. T. Starck, J. Becker, R. Fuhrer, S. Sündermann, J. W. Stark, V. Falk, *Interact. Cardiovasc. Thorac. Surg.* **2014**, *18*, 13.

[5] E. A. Fisher, J. A. Stahl, J. H. Budd, M. E. Goldman, *J. Am. Coll. Cardiol.* **1991**, *18*, 1333.

[6] a) S. H. Little, S. R. Igo, M. McCulloch, C. J. Hartley, Y. Nosé, W. A. Zoghbi, *Ultrasound Med. Biol.* **2008**, *34*, 647; b) S. H. Little, S. R. Igo, B. Pirat, M. McCulloch, C. J. Hartley, Y. Nosé, W. A. Zoghbi, *Am. J. Cardiol.* **2007**, *99*, 1440; c) A. Quaini, S. Canic, G. Guidoboni, R. Glowinski, S. Igo, C. Hartley, W. Zoghbi, S. Little, *Cardiovasc. Eng. Technol.* **2011**, *2*, 77.

[7] T. Blum, S. M. Heining, O. Kutter, N. Navab, Advanced Training Methods Using an Augmented Reality Ultrasound Simulator, presented at ISMAR, Orlando, USA **2009**.

[8] M. Claudon, C. F. Dietrich, B. I. Choi, D. O. Cosgrove, M. Kudo, C. P. Nolsøe, F. Piscaglia, S. R. Wilson, R. G. Barr, M. C. Chammas, *Ultrasound Med. Biol.* **2013**, *39*, 187.

[9] M. Loepfe, Combustion-Driven Actuators, http://softroboticstoolkit.com/book/combustion-driven-actuators, accessed: December, **2014**.

[10] A. Iimura, Y. Nakamura, M. Itoh, *Ann. Anat.* **2003**, *185*, 91.

[11] J. Ophir, K. J. Parker, *Ultrasound Med. Biol.* **1989**, *15*, 319.

[12] F. R. Eirich, *Rheology*, Academic Press, New York, NY, USA **1968**.

[13] T. Ohashi, H. Liu, T. Yamaguchi, in *Clinical Application of Computational Mechanics to the Cardiovascular System*, (Ed: T. Yamaguchi), Springer, Japan **2000**, p. 186.

[14] I. Marshall, S. Zhao, P. Papathanasopoulou, P. Hoskins, X. Y. Xu, *J. Biomech.* **2004**, *37*, 679.

[15] a) G. Camino, S. M. Lomakin, M. Lazzari, *Polymer* **2001**, *42*, 2395; b) M. Loepfe, C. M. Schumacher, U. B. Lustenberger, J. W. Stark, *SoRo* **2015**, DOI: 10.1089/soro.2014.0021.